Identification of a *de novo* mutation in *TLK1* associated with a neurodevelopmental disorder and immunodeficiency

Marina Villamor-Payà[1,2], María Sanchiz-Calvo[1,#], Jordann Smak[2], Lynn Pais[3,4], Malika Sud[4], Uma Shankavaram[2], Alysia Kern Lovgren[4], Christina Austin-Tse[4], , Vijay S Ganesh[4,5], Marina Gay[1], Marta Vilaseca[1], Gianluca Arauz-Garofalo[1], Lluís Palenzuela[1] , Grace VanNoy[3,4,], Anne O'Donnell-Luria[3,4] and Travis H. Stracker[1, 2].

Affiliations

[1]Institute for Research in Biomedicine (IRB Barcelona), The Barcelona Institute of Science and Technology, Barcelona 08028, Spain

[2]National Cancer Institute, Center for Cancer Research, Radiation Oncology Branch, Bethesda, MD 20892, USA.

[3]Division of Genetics & Genomics, Department of Pediatrics, Boston Children's Hospital, Boston, MA 02115, USA.

[4]Program in Medical and Population Genetics, Broad Institute of MIT and Harvard, Cambridge, MA 02142, USA.

[5]Department of Neurology, Brigham and Women's Hospital, Boston, MA 02115, USA.

#Current affiliation: Laboratory for Neurobiology and Gene Therapy, Department of Neurosciences, Leuven Brain Institute, KU Leuven, 3000 Leuven, Belgium

***Lead Contact**: travis.stracker@nih.gov

Running title: *TLK1*-associated neurodevelopmental disorder

Keywords: Neurodevelopmental disorder, microcephaly, immunodeficiency, TLK1, TLK2, STAT3

Abstract

Background

The Tousled-like kinases 1 and 2 (TLK1/TLK2) regulate DNA replication, repair and chromatin maintenance. TLK2 variants are associated with 'Intellectual Disability, Autosomal Dominant 57' (MRD57), a neurodevelopmental disorder (NDD) characterized by intellectual disability (ID), autism spectrum disorder (ASD) and microcephaly. Several TLK1 variants have been reported in NDDs but their functional significance is unknown.

Methods

A male patient presenting with ID, seizures, global developmental delay, hypothyroidism, and primary immunodeficiency was determined to have a novel, heterozygous variant in TLK1 (c.1435C>G, p.Q479E) by genome sequencing (GS). Single cell gel electrophoresis, western blot, flow cytometry and RNA-seq were performed in patient-derived lymphoblast cell lines. In silico, biochemical and proteomic analysis were used to determine the functional impact of the p.Q479E variant and previously reported NDD-associated TLK1 variant, p.M566T.

Results

Transcriptome sequencing in patient-derived cells confirmed expression of TLK1 transcripts carrying the p.Q479E variant and revealed alterations in genes involved in class switch recombination and cytokine signaling. Cells expressing the p.Q479E variant exhibited reduced cytokine responses and higher levels of spontaneous DNA damage but not increased sensitivity to radiation or DNA repair defects. The p.Q479E and p.M566T variants impaired kinase activity but did not strongly alter localization or proximal protein interactions.

Conclusion

Our study provides the first functional characterization of TLK1 variants associated with NDDs and suggests potential involvement in central nervous system and immune system

development. Our results indicate that, like TLK2 variants, TLK1 variants may impact development in multiple tissues and should be considered in the diagnosis of rare NDDs.

Introduction

The Tousled-like kinases 1 and 2 (TLK1 and TLK2) are conserved serine-threonine kinases that function in numerous cellular processes, including DNA replication, DNA repair, transcription and chromatin maintenance(1). Both TLK1 and TLK2 interact with and regulate the ASF1A and ASF1B histone H3-H4 chaperones(2–7). Depletion of both TLK1 and TLK2, or both ASF1A and ASF1B, led to overlapping cellular phenotypes, including DNA damage, innate immune activation and the induction of the alternative lengthening of telomeres (ALT) pathway(8–10). TLK1 and TLK2 are regulated by the DNA damage response and the phosphorylation of TLK1 on its C-terminus by the checkpoint kinase CHK1 inhibits TLK1 activity(11,12). TLK1 also phosphorylates the RAD9 protein, part of the RAD9-RAD1-HUS1 (9-1-1) complex that responds to DNA damage and regulates CHK1 activity, as well as the NEK1 kinase, that is involved in the DNA damage response and ciliogenesis(4,13–19).

Despite clear associations with fundamental cellular processes and multiple links to the DNA damage response, *Tlk1* deficiency in mice did not result in any overt phenotypes. Notably, both immune system development and fertility were grossly normal, suggesting DNA repair-dependent processes in V(D)J recombination and meiosis were functional(8). Additionally, the deletion of *TLK1* in hundreds of cancer cell lines did not strongly influence cell fitness(20). In contrast, loss of *Tlk2* in mice led to embryonic lethality due to a role in placental development, and *TLK2* is an commonly essential gene in many cancer cell lines, indicating distinct functions or regulation that remain to be fully understood(8,20).

Variants in *TLK2* have been implicated in Intellectual Developmental Disorder, Autosomal Dominant 57 (MRD57, MIM# 618050), a heterogenous neurodevelopmental disorder (NDD)

characterized by intellectual disability (ID), autism spectrum disorder (ASD), microcephaly, additional behavioral problems, growth delay and facial dysmorphism, including blepharophimosis, telecanthus, prominent nasal bridge, broad nasal tip, thin vermilion of the upper lip and upslanting palpebral fissures(21–25). A subset of cases also exhibited gastrointestinal problems, seizures, skeletal malformations and ocular problems. With one exception, all of the disease-associated *TLK2* variants identified to date are heterozygous, and those examined biochemically showed diminished kinase activity, suggesting pathological outcomes are largely due to reduced kinase activity(23,24).

Activation of TLK2 requires dimerization through its first coiled-coil (CC1), which is also required for its heterodimerization with TLK1(26,27). As TLK1 and TLK2 interact, some of the identified *TLK2* missense variants may exert dominant negative effects on wild type TLK2 and potentially TLK1(28). While >40 *TLK2* variants have been identified in NDD patients, to date, only four *de novo TLK1* variants have been associated with NDDs (Table 1)(21–25,29). However, no causal links have been established, and the effects of any of the individual variants on protein function have not been investigated.

Here we report the identification of a male proband who presented with microcephaly, ID, seizures, global developmental delay, cerebral calcifications, feeding difficulties, growth hormone deficiency, hypothyroidism, urticaria and primary immunodeficiency. He had extensive prior genetic testing, including whole exome sequencing (WES), that did not identify a clear genetic cause for his phenotype. Subsequent research exome sequencing (ES) and genome sequencing (GS) through the Rare Genomes Project (RGP) identified heterozygous, *de novo* variants in *TLK1* c.1435C>G (p.Q479E) and *MDM1* c.1197dupT (p.K400Ter).

***TLK1* variant**	**TLK1 protein**	**Disease association**	**Reference**

c.74C>T	p.P25L	Intellectual disability	(25)
c.112_113del	p.T38fs	Intellectual disability	ClinVar
c.424G>A	p.R142S	Limb, ear, eye and muscle abnormalities	DECIPHER
c.1101del	p.K367Nfs*	Schizophrenia	(30)
c.1435C>G	p.Q479E	Intellectual disability, microcephaly, immunodeficiency	This study
c.1697T>C	p.M566T	Autism Spectrum Disorder	(29)
c.1796C>G	p.A599G	Congenital heart defect	(31)

Table 1: List of *TLK1* variants reported with links to human disease. Positions are based on NM_012290.5.

Materials and Methods

Genome sequencing (GS), variant calling, and prioritization

GS and data processing for this individual and his parents were performed by the Genomics Platform at the Broad Institute of MIT and Harvard. PCR-free preparation of sample DNA (350 ng input at >2 ng/uL) was accomplished using Illumina HiSeq X Ten v2 chemistry. Libraries were sequenced to a mean target coverage of >30X. WGS data was processed through a pipeline based on Picard, using base quality score recalibration and local realignment at known indels. The BWA aligner was used for mapping reads to the human genome build 38. Single Nucleotide Variants (SNVs) and insertions/deletions (indels) were jointly called across all samples using the Genome Analysis Toolkit (GATK) HaplotypeCaller package version 4.0. Default filters were applied to SNV and indel calls using the GATK Variant Quality Score Recalibration (VQSR) approach. Annotation was performed using Variant Effect Predictor (VEP). GATK-SV(32) was used to detect structural variants (SVs), which were annotated with the GATK SVAnnotate tool. Mitochondrial DNA (mtDNA) single nucleotide and small indel variants were called from GS data using the gnomAD-mitochondria pipeline(33) and large mtDNA deletions were called by MitoSAlt(34). ExpansionHunter v5 was used to genotype known disease-associated short tandem repeats (STRs)(35). Lastly, the variant call set was

uploaded to seqr for analysis by the RGP team. Variants in *TLK1* (p.Gln479Glu) and *MDM1* (p.Lys400Ter) were submitted to ClinVar (submission ID: SUB13580789).

Cell culture and generation of patient cell lines

Peripheral blood mononuclear cells were isolated from whole blood using Histopaque-1077 (Sigma-Aldrich) and subsequently immortalized with Epstein-Barr virus transformation (Coriell Institute). Lymphoblastoid cell lines were cultured in RPMI-1640 medium (Corning) supplemented with 15% fetal bovine serum (FBS) (Gibco), 1% penicillin-streptomycin, and 2 mM L-glutamine. AD-293 cells (Stratagene) were grown in DMEM supplemented with 10% FBS (Sigma-Aldrich), 50 U/mL penicillin and 50 µg/mL streptomycin (Thermo Fisher Scientific) and authenticated using STR testing (ATCC). All cells were kept at 37°C in a 5% CO_2 incubator. Cells were counted with a Countess cell counter (Invitrogen) and viability was assessed using trypan blue. For any given experiment, only cell cultures with a viability >90% were used. Cells were routinely tested for mycoplasma and found negative (Lonza).

Genomic DNA and RNA Purification

Genomic DNA was purified from **lymphoblastoid cell lines** using the Gentra Puregene Cell kit (Qiagen) following manufacturer's instructions. Total RNA was extracted from lymphoblastoid cell lines (LCLs) using the SV Total RNA Isolation System (Promega) following manufacturer's instructions. Full methods provided in **online supplemental materials and methods**.

PCR amplification and DNA extraction from agarose gels

Genomic DNA was subjected to 35 cycles of PCR amplification using Q5 High-Fidelity DNA Polymerase (New England Biolabs) with primers that allow for the amplification of the region containing the variants of interest (**online supplemental table S1).** PCR products were run in a 2% agarose gel and purified using the Nucleospin Gel and PCR clean-up kit (Macherey-

Nagel) following manufacturer's instructions. Full methods provided in **online supplemental materials and methods.**

Nextera library preparation and sequence analysis for variant calling in PCR products

DNA libraries were prepared using the Nextera XT DNA Library Prep kit (Illumina) following manufacturer's instructions. Sequencing of PCR amplicons was carried out using the MiSeq Nano kit sequencing system (Illumina) with 150 bp paired-end (PE) reads. Cleaned reads were obtained by Trim Galore and FASTQ sequences aligned to the hg38 genome build followed by BCFtools for variant calling and alternate allele frequency of the sequenced genes(36). A filter with quality score >=20 was used to remove variants likely observed purely by chance.

RNA sequencing (RNA-seq)

RNA-seq was performed in the CCR Genomics core facility. RNA-seq data processing was performed using the RNA-seq pipelines of the CCBR Pipeliner framework (https://github.com/CCBR/Pipeliner). Full analysis methods provided in **online supplemental materials and methods.** Data was submitted to GEO: GSE241032.

***In silico* prediction and modeling of missense variants**

In silico prediction of variants was analyzed using seqr (https://seqr.broadinstitute.org)(37). Residue conservation was determined using ConSurf (https://consurf.tau.ac.il)(38) and the heatmap generated using Prism. The TLK1 kinase domain structure was generated using Alphafold (https://alphafold.ebi.ac.uk) and color modified in PyMol to indicate residues of interest.

Comet and cell proliferation assays

Comet assays were performed according to manufacturer's instructions (Trevigen). Proliferation was assessed using the Click-iT Plus EdU Flow Cytometry Assay Kit (Invitrogen) following manufacturer's instructions. Full methods provided in **online supplementary materials and methods.**

Cloning, site-directed mutagenesis, transfection, streptavidin affinity purification, western blotting and kinase assays

Cloning, mutagenesis, transfections, western blotting, streptavidin affinity purification of TLK1 from cell lysates and *in vitro* kinase assays were performed as previously described with minor variations(24). Full methods are provided in the online supplemental materials and methods. Primers are provided in **online supplementary table S1,** antibodies are provided in **online supplementary table S2** and uncropped westerns including those used for quantification are shown in **online supplementary figure S1.** Westerns and gels used for kinase assays are shown in **online supplementary figure S2.** Proteomic data is available in the PRIDE repository: PXD019450.

Results

Identification of a proband with a neurodevelopmental disorder and a *de novo TLK1* variant

After an uncomplicated pregnancy, the proband was born with microcephaly noted early in the postnatal period. Between 0-5 months of age, he was admitted to the neonatal intensive care unit (NICU) due to an infection that progressed to respiratory failure. During a several month course in the NICU, he was found to have B- and T-cell deficiency and diagnosed with primary hypothyroidism (TSH 33 uIU/mL, repeat 18.6 uIU/mL). At less than 5 months old, he had a stroke and a generalized seizure and was treated with levetiracetam, after which he was weaned off levetiracetam. Brain MRI revealed symmetric periventricular and subcortical

leukoencephalopathy with mild cystic white matter encephalomalacia, ex vacuo ventriculomegaly, thinning of the corpus callosum, and bilateral optic nerve atrophy (**Figure 1A-D**.

T cells normalized before 5 years of age, but he still has B-cell deficiency and hypogammaglobulinemia (low IgG), treated with weekly subcutaneous immunoglobulin. Enzymatic testing for severe combined immunodeficiency (SCID), including adenosine deaminase (ADA) and purine nucleoside phosphorylase (PNP), was normal (age 0).

Between 15 and 20 months, he had a kidney biopsy following episodes of proteinuria and hematuria that was not diagnostic. Between 6 and 10 years old, he was diagnosed with growth hormone deficiency and treated with growth hormone injections.

His medical history is also notable for significant global developmental delay, hypotonia, mild outer retinal dystrophy, feeding difficulties, and skin findings including poikiloderma, annular urticaria, and a chronic rash that flares up upon infection. He has used a walker for support from 15-20 months of age and has significant speech and language delays, though his receptive abilities are more developed than his expressive language.

The proband had thorough clinical genetic testing, all of which came back normal. This included chromosomal microarray and karyotyping, candidate-gene sequencing (*CIAS1, RAB27A, RECQL4*), targeted mutation analysis (Factor V Leiden p.R506Q, Factor II/prothrombin p.G20210A), mtDNA analysis and nuclear mitochondrial disease panel, and panel testing (SCID panel, Aicardi Gouitéres panel, Noonan syndrome panel, dyskeratosis congenita panel). Clinical exome sequencing (ES) and subsequent ES reanalysis in 2017 were negative.

Research GS done through RGP identified a rare *de novo* frameshift variant in *MDM1* (c.1197dupT; p.Lys400Ter; 12:68315249, hg38) and a rare *de novo* missense variant in *TLK1* (c.1435C>G; p.Gln479Glu; 2:171007045, hg38) further detailed in this report.

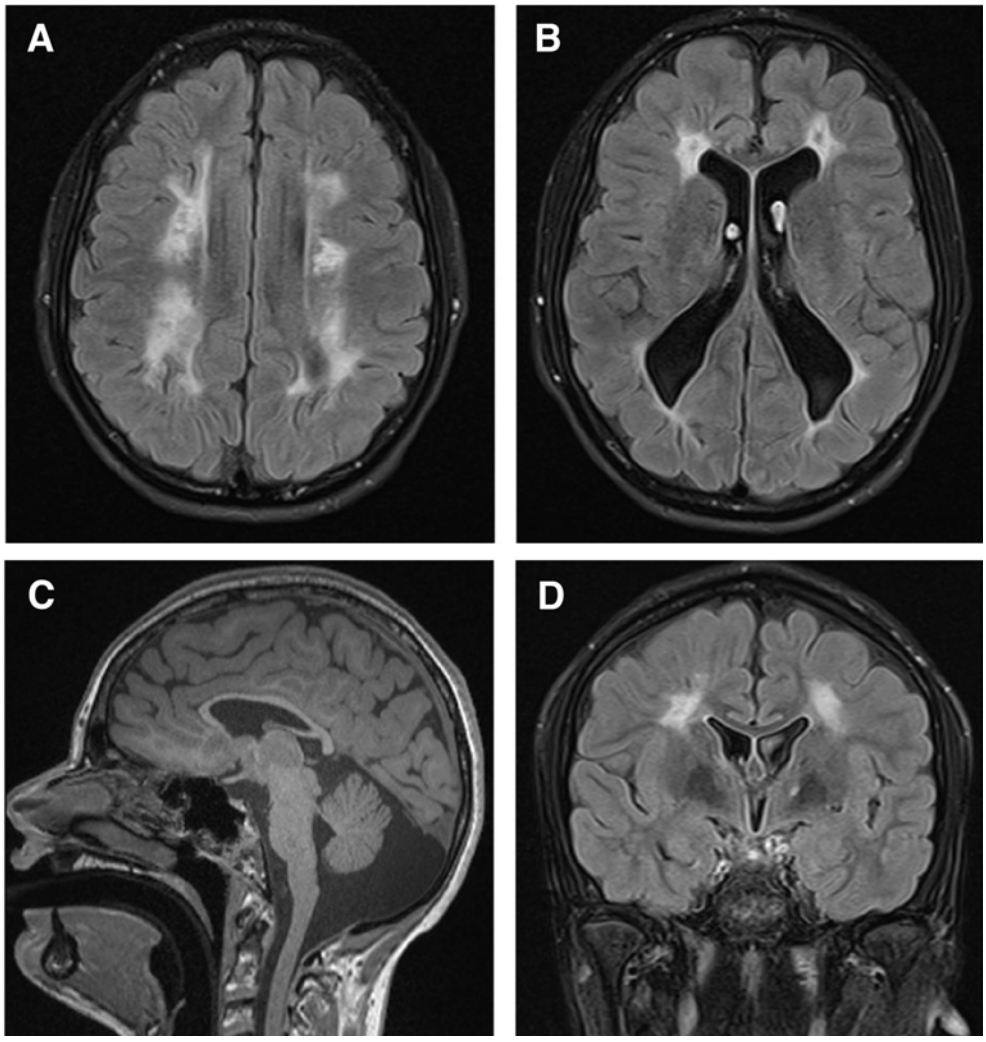

Figure 1: T2/FLAIR axial (A, B), sagittal (C), and coronal (D) sections from age 10-15 years shows symmetric periventricular and subcortical leukoencephalopathy with mild cystic white matter encephalomalacia, ex vacuo ventriculomegaly, and thin corpus callosum.

Characterization of patient-derived cells expressing the *TLK1* and *MDM1* variants

To further investigate the potential impact of the mutations, PBMCs from the proband and an unaffected female sibling of a similar age, were isolated and transformed with Epstein Barr Virus (EBV) to generate lymphoblastoid cell lines (LCLs). Genomic DNA from expanded LCLs was

amplified with specific primers, and sequencing confirmed the presence of both the *TLK1* and *MDM1* variants identified by GS.

We next performed RNA-seq on each LCL to identify differentially expressed genes (DEGs) and assess the expression levels of the specific variant alleles of both *MDM1* and *TLK1*. Both *TLK1* and *MDM1* were expressed to similar levels in each cell line (**Figure 2A and online supplementary table S3**). The allele harboring the *TLK1* variant was transcribed to a similar extent as the wildtype allele (**Figure 2B** and **online supplementary table S4**), and quantitative western blotting showed total TLK1 protein levels slightly elevated in cells from the proband with the p.Q479E variant compared to the unaffected sibling (**Figure 2C**). In contrast to the *TLK1* variant, the *MDM1* mutant allele was not detectably expressed, likely indicating nonsense-mediated RNA decay (NMD) (**Figure 2B**). However, total MDM1 protein levels appeared similar, consistent with RNA-seq data, suggesting that MDM1 protein levels are unaffected in the LCL line (**Figure 2D**). We next examined the phosphorylation of two reported TLK1 substrates ASF1A and NEK1(6,17). In both cases, no significant difference in phosphorylation of either substrate could be observed between the cell lines (**Figure 2E-F**).

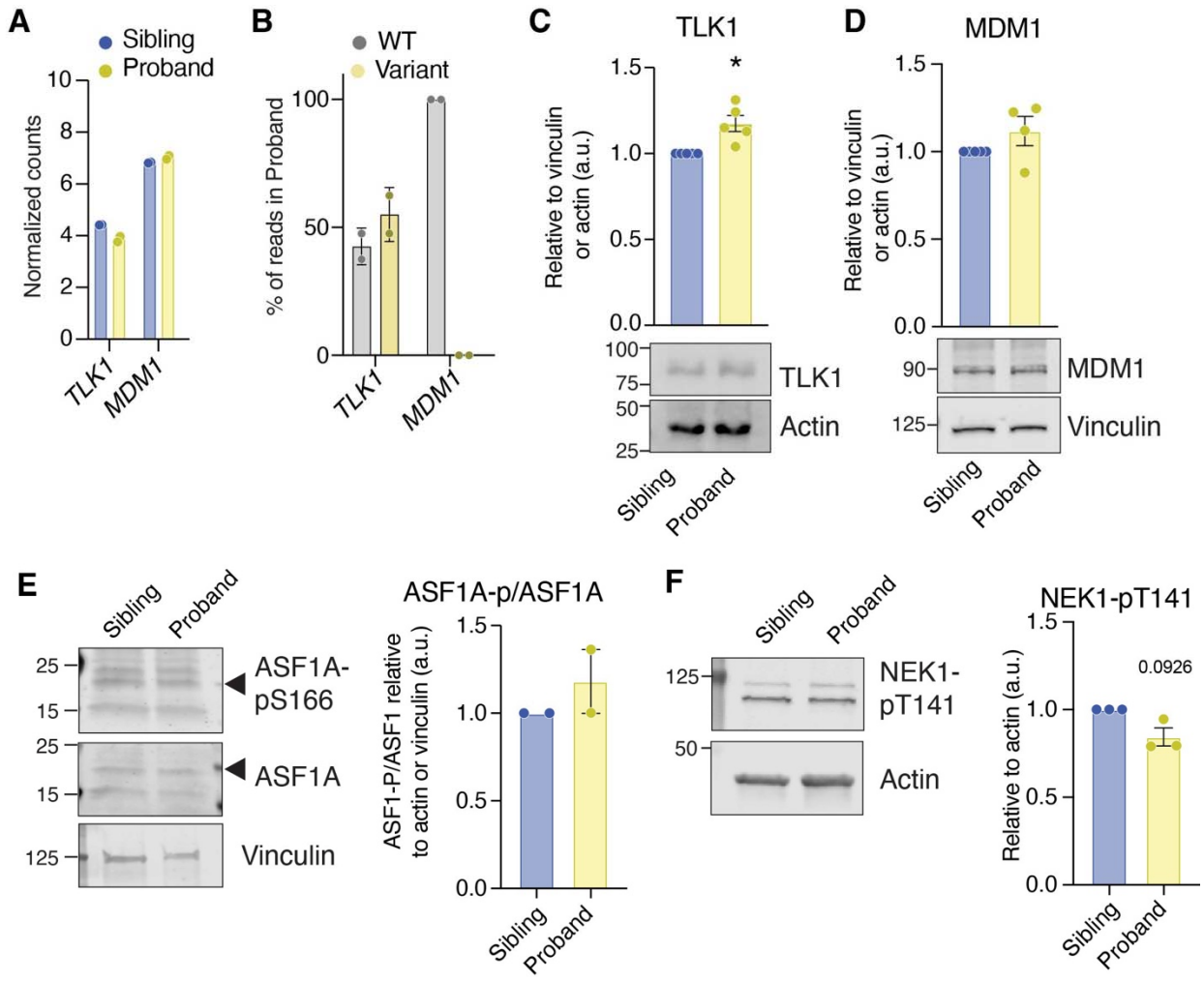

Figure 2: *TLK1* and *MDM1* variant alleles and impact on protein levels. A. Normalized read counts for the indicated genes from RNA-seq of transformed LCLs of the Sibling or Proband. N=2, mean and standard deviation are shown. Full details in **online supplementary table S3**. **B.** Allele specific expression of the indicated genes in the Proband inferred from RNA-seq data. N=2, mean and standard deviation are shown. Full details in **online supplementary table S4.** **C.** Representative blot of protein levels of TLK1. Quantification of western blots (N=5) is shown in right panel normalized to Vinculin or Actin. **D.** Representative blot of protein levels of MDM1 and quantification of western blots (N=4) is shown in right panel normalized to Vinculin or Actin. **E.** Representative blot of ASF1A and ASF1A-pS166 (ASF1A-p) levels and quantification of western blots (N=2) is shown in right panel. **F.** Representative blot NEK1-pS141 (P-NEK1)

levels and quantification of western blots (N=3) is shown in right panel. N represents biological replicates, statistical significance was determined using an unpaired t test with Welch's correction (*P<0.05) in panels C,D.

Gene expression differences consistent with immunodeficiency

RNA-seq data was further analyzed to identify DEGs between the LCL cell lines (**Figure 3A**). Ingenuity pathway analysis (IPA) identified Primary Immunodeficiency Signaling (PID) as a top enriched category, consistent with the immunodeficiency of the proband (**Figure 3A-C**). Many of the genes identified are involved in class switch recombination (CSR), and additional DEGs in CSR genes were identified manually, including CD27 and FCRL3 (**Online supplemental table S3**). In addition, the STAT3 pathway, Osteoarthritis pathway (OSTEO) and Hepatic fibrosis pathways were among the top 4 significantly altered pathways in the LCLs of the proband compared to the sibling (**Figure 3A-C**). Notably, these pathways included a number of transcriptional regulators, cytokines and other cell surface proteins that influence cell to cell interactions in the immune system.

Examination of the STAT3 signaling related genes revealed a number of DEGs, including the Interleukin-6 receptor (IL6R) and CSF2RB, which is a component of multiple cytokine receptors. As mutations in STAT3 and IL6R are associated with distinct immunodeficiency syndromes (39), we analyzed STAT3 signaling in cells treated with IL6 and examined the phosphorylation of Tyrosine 705 (Y705) of STAT3, a marker of its activation. While increased levels of pY705-STAT3 were observed in both samples following IL6 treatment, it was markedly reduced in the proband, indicating reduced sensitivity to IL6 (**Figure 3D**). Together, these data indicated that the cells from the proband showed gene expression changes consistent with immunodeficiency and defective CSR and were less responsive to IL6 cytokine stimulation.

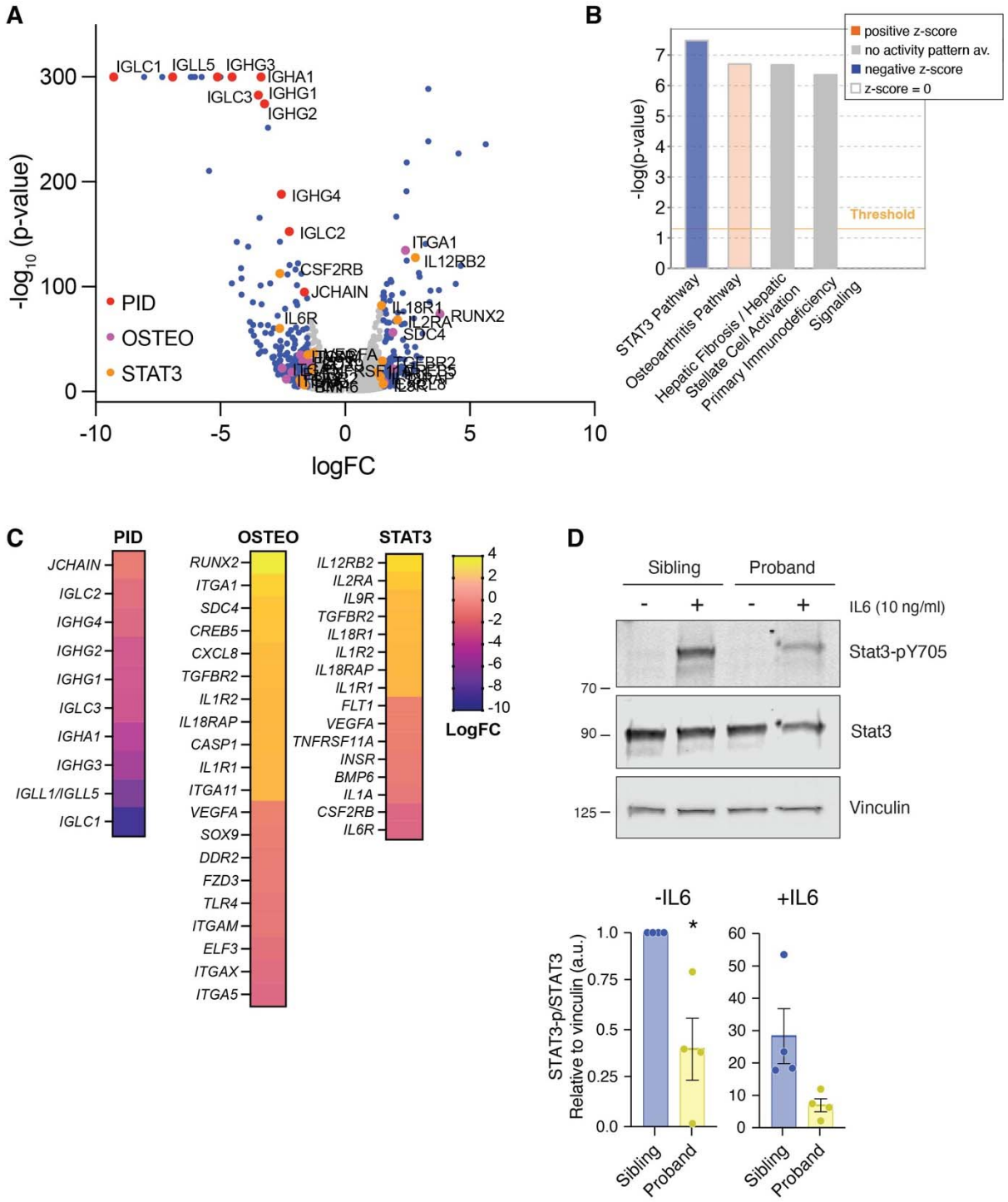

Figure 3: Gene expression differences identify defects in STAT3 signaling in patient-derived cell lines. A. Volcano plot of RNA-seq data depicting DEGs in the Proband compared to Sibling LCLs. Duplicate samples from each LCL line were analyzed. Full data in **online**

306 **supplemental Table S3**. Genes in each enriched category identified in IPA analysis (B) are
307 shown in the indicated color. Hepatic fibrosis genes overlap with Osteoarthritis and are therefore
308 not shown. **B.** Ingenuity Pathway Analysis (IPA) of RNA-seq data is shown. **C.** Heatmap of
309 individual genes from the indicated enriched pathway are shown. **D.** Analysis of STAT3
310 phosphorylation on Y705 in response to IL6 in LCLs. Quantification of 4 independent
311 experiments is shown below the western blot. STAT3-p (Y705)/STAT3 was normalized to
312 vinculin and samples were normalized to Sibling -IL6. Statistical significance was determined
313 using an unpaired t test with Welch's correction (*P<0.05).
314
315 **Growth defects and increased DNA damage in a patient-derived cell line**
316 To determine the potential impact of the genetic variants and DEGs on cell growth and viability,
317 we compared the growth of the proband- and sibling-derived cell lines by plating the same
318 number of live cells and counting them every 24 hours over 72 hours. Viability at the beginning
319 of the experiment was always >90%. The proband-derived cells showed reduced growth over
320 72 hours, with observable differences after 48 hours (**Figure 4A**). Flow cytometry analysis of
321 EdU-pulsed cultures showed a reduction of cells in S-phase with a compensatory increase in
322 the G1 population (**Figure 4B and 4C**). Both the G2/M and sub-G1 populations were also
323 increased in cells from the proband (Figure 4B and 4C). As this suggested potential activation of
324 cell cycle checkpoints, we examined p53 and p21 levels and found that both were upregulated
325 in the proband compared to the unaffected sibling (**Figure 4D and 4E**).
326
327 As the increased p53/p21 levels and elevated sub-G1 population suggested stress or DNA
328 damage signaling, we used the alkaline comet assay to examine the LCLs for spontaneous
329 DNA damage and to examine DNA repair following exposure to 2 Gy ionizing radiation (IR). The
330 proband-derived cells showed increased tail moment values in the alkaline comet assay in the
331 absence of IR treatment, indicating elevated levels of DNA damage (**Figure 4F and 4G**).

However, examination using the neutral comet assay did not reveal evidence of increased DNA strand breaks (**Figure 4H**). Consistent with an absence in DSB repair defects, comets induced by IR treatment were resolved similarly to those in the control cell line, indicating that overall DSB repair was functional, suggesting that spontaneous damage may be ssDNA gaps or base damage (**Figure 4G**).

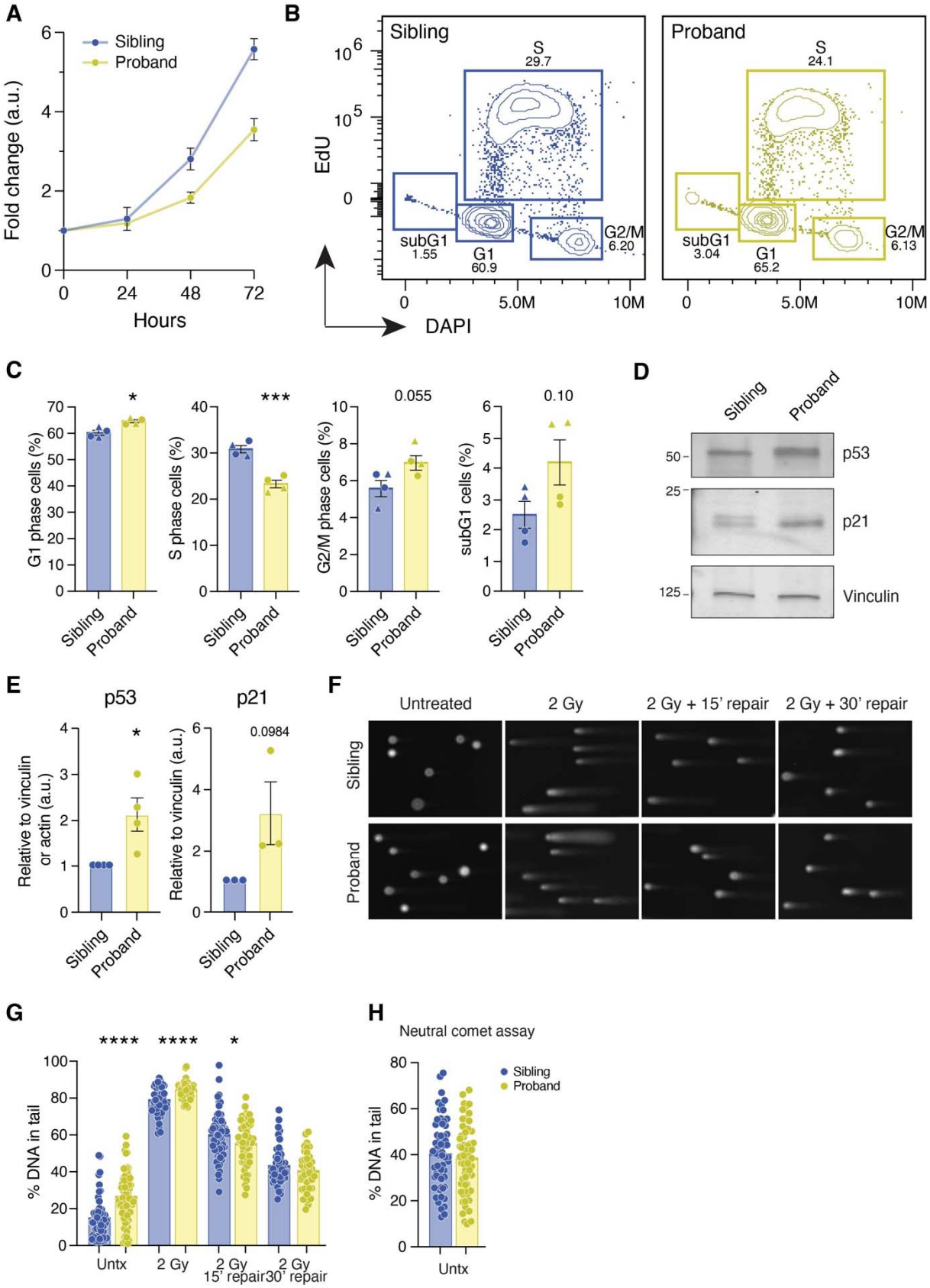

Figure 4: Analysis of cell cycle and DNA damage in patient cell lines. A. Relative cell growth of the Proband and Sibling LCLs. N=6. **B.** Example of representative flow cytometry data to analyze cell cycle in LCLs. Cells were pulsed with 10 μM EdU for 1 hour and stained with DAPI for DNA content. **C.** Quantification of cell cycle phases from N=2 independent experiments with 2 biological replicates each. Replicates from same experiment indicated with a triangle or circle. **D.** Western blot analysis of p53 and p21 levels in LCLs. **E.** Quantification of p53 (N=4) and p21 (N=3) levels from biological replicates. **F.** Representative images of alkaline comet assays untreated or treated with the indicated dose of ionizing radiation (IR). **G.** Analysis of tail moment with the indicated treatments and recovery times. Representative of N=2 independent experiments. **H.** Analysis of tail moment in neutral comet assays. Representative of N=2 independent experiments. At least 100 comets were analyzed per condition and experiment. Statistical significance was determined using an unpaired t test with Welch's correction (****P<0.0001, ***P<0.001, **P<0.01, *P<0.05).

In silico and biochemical analysis of the *TLK1* variant

As the *TLK1* variant was the best genetic candidate for the observed phenotypes, we analyzed it with a variety of prediction tools to determine if the variant was potentially damaging to TLK1 activity (37). The results were variable, with some prediction tools indicating that the variant was damaging and others indicating it was tolerated (**online supplementary table S5).** Analysis of missense constraint (www.decipher.com) indicated that the kinase domain of TLK1 is highly constrained (**online supplementary figure S3**). We next analyzed the specific conservation of the Q479 residue using Consurf, including also an additional *TLK1* variant that was previously reported in a patient with ASD, p.M566T (Table 1)(29,38). Both residues are located within the kinase domain of TLK1, with Q479 located in a beta sheet of the N-lobe and M566 in an alpha helix of the C-lobe. Both residues scored as highly conserved, indicating that they could be important for kinase activity (**Figure 5A**).

365

366 To directly determine if kinase activity was affected, the p.Q479E or p.M566T variants were
367 generated in an expression vector using site-directed mutagenesis. N-terminally Strep-FLAG-
368 tagged TLK1-WT, or the two variants, were expressed in AD-293 cells and affinity purified from
369 cell lysates for *in vitro* kinase assays using purified ASF1A as a substrate (**Figure 5B**). A kinase
370 dead mutant of TLK2 (D592V) was used as a negative control for non-specific labeling of the
371 substrate(24). Both the p.Q479E and p.M566T variant proteins showed reduced
372 autophosphorylation activity compared to TLK1-WT and their kinase activity was impaired to
373 similar extent as TLK2-KD compared to TLK1-WT (**Figures 5B-C**). These results indicated that
374 both variants resulted in severely impaired TLK1 kinase activity.

375

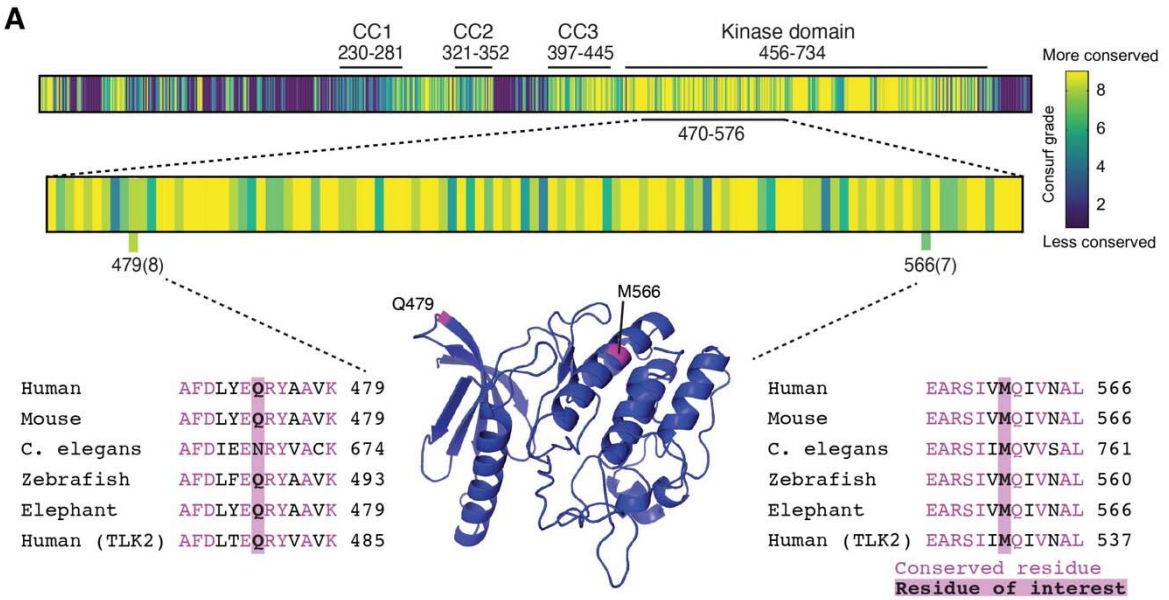

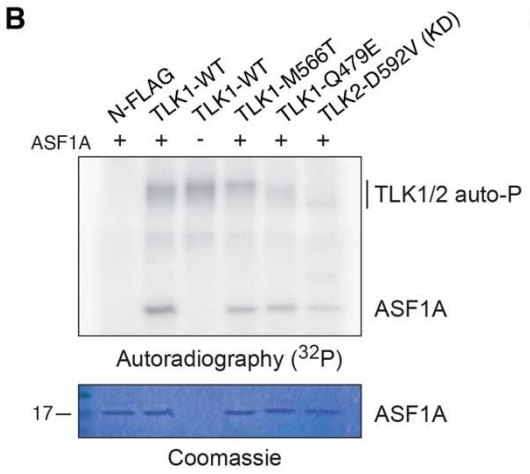

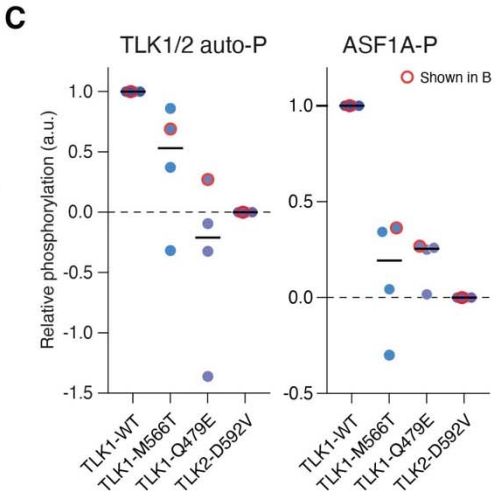

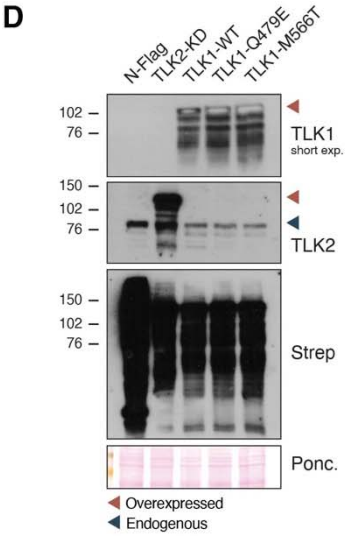

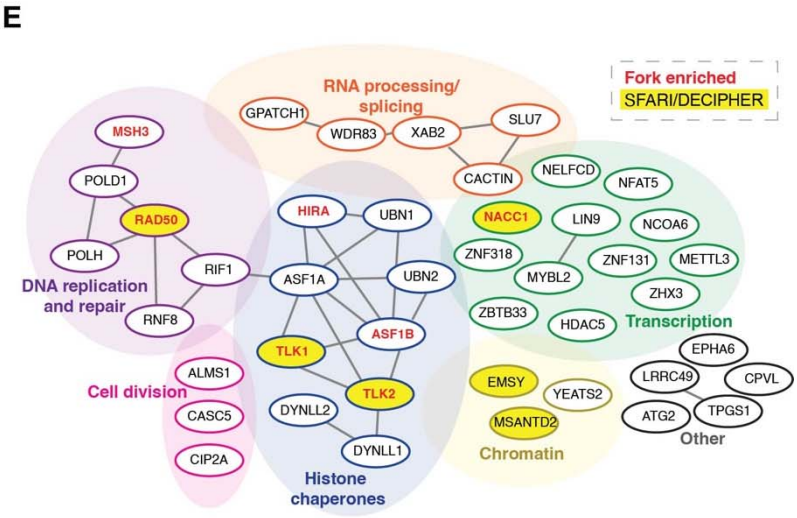

Figure 5: Conservation analysis, kinase activity and proximal interactions of NDD associated TLK1 variants. A. Consurf was used to analyze the level of conservation of the amino acids of human TLK1, with both Q479 and M566 scoring as highly conserved. The predicted structure of the TLK1 kinase domain (Alphafold) is shown with the location of the two residues highlighted in pink(42,43). **B.** Representative *in vitro* kinase assay of Streptavidin purified TLK1-WT or NDD variants on purified ASF1A. TLK2-KD is used as a negative control. **C.** Quantification of N=4 independent kinase assay experiments. **D.** Western blotting of transfected BioID constructs and biotin labeling imaged with Streptavidin. Ponceau is provided as a transfer control. **E.** Network depiction of the proximal interactors identified with TLK1 with physical interactions indicated by solid lines. Proteins identified on nascent DNA at replication forks by iPOND-MS and proteins in the Simon's Foundation Autism Research Initiative (SFARI) or DECIPHER databases are indicated(44). Full results provided in **online supplementary table S6** and additional data in **online supplementary figure S4.**

The NDD-associated TLK1 variants do not strongly alter the proximal proteome

We next examined the proximal proteomes of the TLK1 variants using BioID-MS. The BioID enzyme was fused to the N-terminus of the wild type (WT), p.Q479E and p.M566T constructs, and they were expressed by transient transfection in AD293 cells that were pulsed with biotin for 24 hours (**Figure 5D**)(40). Cells were harvested and biotinylated proteins purified using Streptavidin beads. Isolated proteins were subjected to mass spectrometry and analyzed using SAINTexpress to identify proteins specifically labeled by TLK1-WT or either variant allele (**online supplementary table S6**)(41). The overall network of proximal interactors identified was similar to that we previously observed for TLK2 (**Figure 5E and online supplementary figure S4**)(24). Few strong differences in proximal interactors with either p.Q479E and p.M566T were identified, including with substrates ASF1A and ASF1B, or DYNLL1/LC8, which we previously identified as a robust interactor of TLK2 (**online supplementary figure S4 and table**

403 **S6**) (8) (24). These results indicated that while both TLK1 variants had reduced activity, their
404 proximal interactions were not strongly altered, in contrast to what was observed with several
405 TLK2 NDD variants we previously reported(24).
406
407 **Discussion**
408 In this report we describe a proband with a complex phenotype including developmental delay,
409 intellectual disability, leukoencephalopathy, and primary immunodeficiency. Genetic testing
410 identified potential candidate genes, including *TLK1* and *MDM1*. The *MDM1* variant was not
411 detectable in LCLs, but total *MDM1* expression levels did not appear to be strongly altered at
412 the mRNA or protein level (**Figure 2**). However, we cannot rule out a potential impact of *MDM1*
413 haploinsufficiency in other tissues. In mice, a homozygous truncation mutation of *Mdm1* was
414 linked to retinal degeneration(45). Therefore, the optic nerve atrophy or retinal dystrophy
415 observed in the proband could reflect defects in MDM1 function due to heterozygous expression
416 of the truncated allele or haploinsufficiency in eye development. However, we suggest that
417 *TLK1* is the most likely genetic contributor to the overall phenotype, particularly the
418 neurodevelopmental outcomes.
419
420 While TLK1-deficient mice do not exhibit any obvious developmental phenotypes, ample
421 evidence exists that kinase dead forms of TLK1 may impact the function of TLK1 or TLK2
422 through heterodimerization via the CC1 motif, resulting in a dominant negative effect(26–28).
423 We examined several substrates of TLK1, ASF1A and NEK1, and did not find a clear difference
424 in their phosphorylation in patient-derived cell lines (**Figure 2**). However, cells exhibited
425 significant levels of spontaneous DNA damage and growth defects (**Figure 4**), indicating
426 potential effects on other substrates that we did not analyze in this study. Recent work identified
427 RAD54, a protein involved in homologous recombination of DSBs, as a TLK1 substrate(46).
428 However, the increased DNA damage we observed was not DSBs. TLK1 BioID identified two

proteins involved in Mismatch Repair (MMR), MSH3 and POLD1, as proximal interactors (**Figure 5**). The MMR pathway is involved in the repair of some types of base damage, including that caused by elevated reactive oxygen species, and is also required for CSR(47,48). Thus, TLK1 could potentially play an undefined regulatory role in MMR that is compromised by the variant allele.

Immunodeficiency has not been reported in mouse models of TLK1 or TLK2 deficiency and is therefore hard to directly link to the heterozygous *TLK1* variant identified in this patient based on current knowledge(8). The immunological presentation, as well as the RNA-seq data generated from PBMCs and LCLs, is consistent with defects in lymphocyte maturation, particularly in B-cells, reflecting the proband's status (**Figure 3**). While the proband initially presented with primary immunodeficiency, T-cells recovered, indicating that remaining issues may be the result of impaired B-cell maturation. CSR is a B-cell specific process that is dependent on a number of non-homologous end-joining (NHEJ) pathway genes that largely, but do not completely, overlap with those required for V(D)J recombination(49). A particular feature of CSR is a distinct requirement for 53BP1 and RIF1 that work with a number of proteins to prevent resection and enforce NHEJ(50). Recent work directly linked ASF1 to RIF1-dependent NHEJ DNA repair(51–53). We, and others, have identified RIF1 as a proximal interactor with TLK1 and TLK2 (8,52–54). Thus, defects in TLK1 that influence ASF1 function in this pathway could potentially impact CSR. Further work remains to determine how important TLK-mediated regulation of ASF1 is to RIF1-dependent NHEJ in the context of CSR or if other key repair proteins are regulated by TLK1.

The STAT3 signaling pathway is important for immune system development and emerged as a clearly enriched pathway in our analysis of RNA-seq data. We demonstrated that LCLs are less responsive to IL6 stimulation, likely due to a reduction in IL6R levels (**Figure 3**). Whether this is

a direct result of the TLK1 mutation or reflects the proband's immunodeficient status, we cannot determine for certain. However, it is notable that a number of other signaling pathways are not perturbed, including the phosphorylation of two reported substrates, ASF1A and NEK1 (**Figure 2**), as well as PKC signaling that has been previously linked with neurodevelopmental disorders (**Supplementary Figure S5**)(55). Thus, we postulate that alterations in the STAT3 pathway could potentially contribute to the immune system phenotypes.

In a previous study of *TLK2* variants implicated in MRD57, we observed altered proximal interactions and partial mislocalization of TLK2 variant proteins. In contrast, we did not observe that with either *TLK1* variant, as both showed a very similar repertoire of proximal interactors compared to WT. This suggests potential differences in TLK1 and TLK2 regulation that remain to be further explored. Despite this, the proximal interaction profiles of TLK1 and TLK2 were highly similar, further supporting the proposition that they have a large degree of redundancy (**Figure 5**)(8). As *TLK2* mutations clearly impact neurodevelopment, we propose that the p.Q479E variant likely interferes with overall TLK1-TLK2 activity via homo and heterodimerization that impairs chromatin maintenance during brain development. Further analysis of the neurodevelopmental phenotypes of TLK1- and TLK2-deficient mice is therefore warranted.

In summary, our data strongly indicates that mutations in *TLK1* are likely to be relevant to rare NDDs and should be considered in clinical diagnostics. Further, TLK1, and potentially TLK2, may impact immune system development in certain contexts and additional work is needed to understand their cellular and developmental roles.

Data availability statement

Data are available in public, open access repositories GEO (https://www.ncbi.nlm.nih.gov/geo/) ClinVar (https://www.ncbi.nlm.nih.gov/clinvar/) and PRIDE (https://www.ebi.ac.uk/pride/), included in the article or uploaded as supplementary information.

Ethics approval

The study protocol was approved by the Mass General Brigham Institutional Review Board and informed consent was obtained from the participating family.

Acknowledgements

We thank the Stracker lab and L. Deriano for helpful discussions, S. Khurana for antibody optimization, A. De Benedetti for the kind gift of p-NEK1 antibody, D. Zafra and J. Motley for collaboration agreement support, and the IRB Barcelona mass spectrometry core facility and the CCR Genomics facility for technical support. Thank you to the RGP and Broad Institute Center for Mendelian Genomics teams, particularly Melanie O'Leary and Heidi Rehm for project leadership, Ben Weisburd for tandem repeat analysis, Sarah Stenton for mitochondrial genome analysis, and Alba Sanchis-Juan, Harrison Brand, and Michael Talkowski for structural variant analysis.

Funding: M.V-P. was funded by an FPI fellowship from the Ministry of Science, Innovation and Universities (MCIU: BFU2015-68354-P), T.H.S. was funded by the MCIU (PGC2018-095616-B-I00), the 2017 SGR 1089 (AGAUR), FEDER, the Centres of Excellence Severo Ochoa award and the CERCA Programme. M.S.-C. was supported by the IRB Barcelona. T.H.S, M.V-P, J.S. and U.S. were funded by the NIH Intramural Research Program, National Cancer Institute Center for Cancer Research. Sequencing and analysis were provided by the Broad Institute of MIT and Harvard Rare Genomes Project (RGP) and were funded by the National Human

Genome Research Institute grants UM1 HG008900 (with additional support from the National Eye Institute, and the National Heart, Lung and Blood Institute), U01 HG0011755, and R01 HG009141 and in part by grant number 2020-224274 from the Chan Zuckerberg Initiative DAF, an advised fund of Silicon Valley Community Foundation. V.S.G. is supported by NIH NHGRI T32 (#1T32HG010464).

Competing interests: none declared.

Supplemental Material:

Supplementary materials and methods.

Supplementary Figures

Figure S1: Uncropped western blots.

Figure S2: Uncropped western blots and gels from kinase assays and BioID.

Figure S3: Decipher analysis of TLK2.

Figure S4: BioID-western blot analysis and results comparisons.

Figure S5: Western blotting of PKC substrates.

Supplementary Tables

Table S1: Primers used in this study.

Table S2: Antibodies used in this study.

Table S3: Differentially expressed genes and IPA analysis (excel).

Table S4: Analysis of gene specific SNPs in RNA-seq data.

Table S5: Seqr analysis of the *TLK1* mutation.

Table S6: BioID-MS data of TLK1 and NDD variants (excel).

Bibliography

1. Segura-Bayona S, Stracker TH. The Tousled-like kinases regulate genome and epigenome stability: implications in development and disease. Cell Mol Life Sci. 2019 Jul 13;
2. Silljé HH, Nigg EA. Identification of human Asf1 chromatin assembly factors as substrates of Tousled-like kinases. Curr Biol. 2001 Jul 10;11(13):1068–73.
3. Pilyugin M, Demmers J, Verrijzer CP, Karch F, Moshkin YM. Phosphorylation-mediated control of histone chaperone ASF1 levels by Tousled-like kinases. PLoS One. 2009 Dec 16;4(12):e8328.
4. Canfield C, Rains J, De Benedetti A. TLK1B promotes repair of DSBs via its interaction with Rad9 and Asf1. BMC Mol Biol. 2009 Dec 20;10:110.
5. De Benedetti A. Tousled kinase TLK1B mediates chromatin assembly in conjunction with Asf1 regardless of its kinase activity. BMC Res Notes. 2010 Mar 11;3:68.
6. Klimovskaia IM, Young C, Strømme CB, Menard P, Jasencakova Z, Mejlvang J, et al. Tousled-like kinases phosphorylate Asf1 to promote histone supply during DNA replication. Nat Commun. 2014 Mar 6;5:3394.
7. Simon B, Lou HJ, Huet-Calderwood C, Shi G, Boggon TJ, Turk BE, et al. Tousled-like kinase 2 targets ASF1 histone chaperones through client mimicry. Nat Commun. 2022 Feb 8;13(1):749.
8. Segura-Bayona S, Knobel PA, González-Burón H, Youssef SA, Peña-Blanco A, Coyaud É, et al. Differential requirements for Tousled-like kinases 1 and 2 in mammalian development. Cell Death Differ. 2017 Jul 14;24(11):1872–85.
9. Lee S-B, Segura-Bayona S, Villamor-Payà M, Saredi G, Todd MAM, Attolini CS-O, et al. Tousled-like kinases stabilize replication forks and show synthetic lethality with checkpoint and PARP inhibitors. Sci Adv. 2018 Aug 8;4(8):eaat4985.
10. Segura-Bayona S, Villamor-Payà M, Attolini CS-O, Koenig LM, Sanchiz-Calvo M, Boulton SJ, et al. Tousled-Like Kinases Suppress Innate Immune Signaling Triggered by Alternative Lengthening of Telomeres. Cell Rep. 2020 Aug 4;32(5):107983.
11. Krause DR, Jonnalagadda JC, Gatei MH, Sillje HHW, Zhou B-B, Nigg EA, et al. Suppression of Tousled-like kinase activity after DNA damage or replication block requires ATM, NBS1 and Chk1. Oncogene. 2003 Sep 4;22(38):5927–37.
12. Groth A, Lukas J, Nigg EA, Silljé HHW, Wernstedt C, Bartek J, et al. Human Tousled like kinases are targeted by an ATM- and Chk1-dependent DNA damage checkpoint. EMBO J. 2003 Apr 1;22(7):1676–87.
13. Kelly R, Davey SK. Tousled-like kinase-dependent phosphorylation of Rad9 plays a role in cell cycle progression and G2/M checkpoint exit. PLoS One. 2013 Dec 20;8(12):e85859.
14. Awate S, De Benedetti A. TLK1B mediated phosphorylation of Rad9 regulates its nuclear/cytoplasmic localization and cell cycle checkpoint. BMC Mol Biol. 2016 Feb 9;17:3.
15. Sunavala-Dossabhoy G, De Benedetti A. Tousled homolog, TLK1, binds and

phosphorylates Rad9; TLK1 acts as a molecular chaperone in DNA repair. DNA Repair (Amst). 2009 Jan 1;8(1):87–102.

16. Singh V, Jaiswal PK, Ghosh I, Koul HK, Yu X, De Benedetti A. The TLK1-Nek1 axis promotes prostate cancer progression. Cancer Lett. 2019 Jul 1;453:131–41.
17. Singh V, Connelly ZM, Shen X, De Benedetti A. Identification of the proteome complement of humanTLK1 reveals it binds and phosphorylates NEK1 regulating its activity. Cell Cycle. 2017 May 19;16(10):915–26.
18. Liu S, Ho CK, Ouyang J, Zou L. Nek1 kinase associates with ATR-ATRIP and primes ATR for efficient DNA damage signaling. Proc Natl Acad Sci USA. 2013 Feb 5;110(6):2175–80.
19. Chen Y, Chen C-F, Riley DJ, Chen P-L. Nek1 kinase functions in DNA damage response and checkpoint control through a pathway independent of ATM and ATR. Cell Cycle. 2011 Feb 15;10(4):655–63.
20. Meyers RM, Bryan JG, McFarland JM, Weir BA, Sizemore AE, Xu H, et al. Computational correction of copy number effect improves specificity of CRISPR-Cas9 essentiality screens in cancer cells. Nat Genet. 2017 Dec;49(12):1779–84.
21. Reijnders MRF, Miller KA, Alvi M, Goos JAC, Lees MM, de Burca A, et al. De Novo and Inherited Loss-of-Function Variants in TLK2: Clinical and Genotype-Phenotype Evaluation of a Distinct Neurodevelopmental Disorder. Am J Hum Genet. 2018 Jun 7;102(6):1195–203.
22. Woods E, Spiller M, Balasubramanian M. Report of two children with global developmental delay in association with de novo TLK2 variant and literature review. Am J Med Genet A. 2021 Nov 25;
23. Töpf A, Oktay Y, Balaraju S, Yilmaz E, Sonmezler E, Yis U, et al. Severe neurodevelopmental disease caused by a homozygous TLK2 variant. Eur J Hum Genet. 2020 Mar;28(3):383–7.
24. Pavinato L, Villamor-Payà M, Sanchiz-Calvo M, Andreoli C, Gay M, Vilaseca M, et al. Functional analysis of TLK2 variants and their proximal interactomes implicates impaired kinase activity and chromatin maintenance defects in their pathogenesis. J Med Genet. 2020 Dec 15;
25. Lelieveld SH, Reijnders MRF, Pfundt R, Yntema HG, Kamsteeg E-J, de Vries P, et al. Meta-analysis of 2,104 trios provides support for 10 new genes for intellectual disability. Nat Neurosci. 2016 Sep;19(9):1194–6.
26. Roe JL, Durfee T, Zupan JR, Repetti PP, McLean BG, Zambryski PC. TOUSLED is a nuclear serine/threonine protein kinase that requires a coiled-coil region for oligomerization and catalytic activity. J Biol Chem. 1997 Feb 28;272(9):5838–45.
27. Mortuza GB, Hermida D, Pedersen A-K, Segura-Bayona S, López-Méndez B, Redondo P, et al. Molecular basis of Tousled-Like Kinase 2 activation. Nat Commun. 2018 Jun 28;9(1):2535.
28. Sunavala-Dossabhoy G, Li Y, Williams B, De Benedetti A. A dominant negative mutant of TLK1 causes chromosome missegregation and aneuploidy in normal breast epithelial cells. BMC Cell Biol. 2003 Oct 28;4:16.
29. De Rubeis S, He X, Goldberg AP, Poultney CS, Samocha K, Cicek AE, et al. Synaptic, transcriptional and chromatin genes disrupted in autism. Nature. 2014 Nov 13;515(7526):209–15.
30. Fromer M, Pocklington AJ, Kavanagh DH, Williams HJ, Dwyer S, Gormley P, et al. De novo mutations in schizophrenia implicate synaptic networks. Nature. 2014 Feb 13;506(7487):179–84.
31. Homsy J, Zaidi S, Shen Y, Ware JS, Samocha KE, Karczewski KJ, et al. De novo mutations in congenital heart disease with neurodevelopmental and other congenital anomalies. Science. 2015 Dec 4;350(6265):1262–6.
32. Collins RL, Brand H, Karczewski KJ, Zhao X, Alföldi J, Francioli LC, et al. A structural

variation reference for medical and population genetics. Nature. 2020 May 27;581(7809):444–51.
33. Laricchia KM, Lake NJ, Watts NA, Shand M, Haessly A, Gauthier L, et al. Mitochondrial DNA variation across 56,434 individuals in gnomAD. Genome Res. 2022 Mar;32(3):569–82.
34. Basu S, Xie X, Uhler JP, Hedberg-Oldfors C, Milenkovic D, Baris OR, et al. Accurate mapping of mitochondrial DNA deletions and duplications using deep sequencing. PLoS Genet. 2020 Dec 14;16(12):e1009242.
35. Dolzhenko E, van Vugt JJFA, Shaw RJ, Bekritsky MA, van Blitterswijk M, Narzisi G, et al. Detection of long repeat expansions from PCR-free whole-genome sequence data. Genome Res. 2017 Nov;27(11):1895–903.
36. Danecek P, McCarthy SA. BCFtools/csq: haplotype-aware variant consequences. Bioinformatics. 2017 Jul 1;33(13):2037–9.
37. Pais LS, Snow H, Weisburd B, Zhang S, Baxter SM, DiTroia S, et al. seqr: A web-based analysis and collaboration tool for rare disease genomics. Hum Mutat. 2022 Jun;43(6):698–707.
38. Ashkenazy H, Abadi S, Martz E, Chay O, Mayrose I, Pupko T, et al. ConSurf 2016: an improved methodology to estimate and visualize evolutionary conservation in macromolecules. Nucleic Acids Res. 2016 Jul 8;44(W1):W344-50.
39. Spencer S, Köstel Bal S, Egner W, Lango Allen H, Raza SI, Ma CA, et al. Loss of the interleukin-6 receptor causes immunodeficiency, atopy, and abnormal inflammatory responses. J Exp Med. 2019 Sep 2;216(9):1986–98.
40. Kim DI, Jensen SC, Noble KA, Kc B, Roux KH, Motamedchaboki K, et al. An improved smaller biotin ligase for BioID proximity labeling. Mol Biol Cell. 2016 Apr 15;27(8):1188–96.
41. Teo G, Liu G, Zhang J, Nesvizhskii AI, Gingras A-C, Choi H. SAINTexpress: improvements and additional features in Significance Analysis of INTeractome software. J Proteomics. 2014 Apr 4;100:37–43.
42. Varadi M, Anyango S, Deshpande M, Nair S, Natassia C, Yordanova G, et al. AlphaFold Protein Structure Database: massively expanding the structural coverage of protein-sequence space with high-accuracy models. Nucleic Acids Res. 2022 Jan 7;50(D1):D439–44.
43. Jumper J, Evans R, Pritzel A, Green T, Figurnov M, Ronneberger O, et al. Highly accurate protein structure prediction with AlphaFold. Nature. 2021 Aug;596(7873):583–9.
44. Wessel SR, Mohni KN, Luzwick JW, Dungrawala H, Cortez D. Functional analysis of the replication fork proteome identifies BET proteins as PCNA regulators. Cell Rep. 2019 Sep 24;28(13):3497–3509.e4.
45. Chang B, Mandal MNA, Chavali VRM, Hawes NL, Khan NW, Hurd RE, et al. Age-related retinal degeneration (arrd2) in a novel mouse model due to a nonsense mutation in the Mdm1 gene. Hum Mol Genet. 2008 Dec 15;17(24):3929–41.
46. Ghosh I, Kwon Y, Shabestari AB, Chikhale R, Chen J, Wiese C, et al. TLK1-mediated RAD54 phosphorylation spatio-temporally regulates Homologous Recombination Repair. Nucleic Acids Res. 2023 Jul 13;
47. Schrader CE, Edelmann W, Kucherlapati R, Stavnezer J. Reduced isotype switching in splenic B cells from mice deficient in mismatch repair enzymes. J Exp Med. 1999 Aug 2;190(3):323–30.
48. Ehrenstein MR, Neuberger MS. Deficiency in Msh2 affects the efficiency and local sequence specificity of immunoglobulin class-switch recombination: parallels with somatic hypermutation. EMBO J. 1999 Jun 15;18(12):3484–90.
49. Saha T, Sundaravinayagam D, Di Virgilio M. Charting a DNA repair roadmap for immunoglobulin class switch recombination. Trends Biochem Sci. 2021 Mar;46(3):184–99.

50. Zimmermann M, de Lange T. 53BP1: pro choice in DNA repair. Trends Cell Biol. 2014 Feb;24(2):108–17.
51. Lee KY, Im J-S, Shibata E, Dutta A. ASF1a Promotes Non-homologous End Joining Repair by Facilitating Phosphorylation of MDC1 by ATM at Double-Strand Breaks. Mol Cell. 2017 Oct 5;68(1):61–75.e5.
52. Tang M, Chen Z, Wang C, Feng X, Lee N, Huang M, et al. Histone chaperone ASF1 acts with RIF1 to promote DNA end-joining in BRCA1-deficient cells. J Biol Chem. 2022 Apr 23;101979.
53. Feng S, Ma S, Li K, Gao S, Ning S, Shang J, et al. RIF1-ASF1-mediated high-order chromatin structure safeguards genome integrity. Nat Commun. 2022 Feb 17;13(1):957.
54. Sukackaite R, Cornacchia D, Jensen MR, Mas PJ, Blackledge M, Enervald E, et al. Mouse Rif1 is a regulatory subunit of protein phosphatase 1 (PP1). Sci Rep. 2017 May 18;7(1):2119.
55. Callender JA, Newton AC. Conventional protein kinase C in the brain: 40 years later. Neuronal Signal. 2017 Apr 10;1(2):NS20160005.